JAAS

Spatial and Temporal Distribution of Metal Atoms and their Diatomic Oxide Molecules in Femtosecond Laser-Induced Plasmas

Journal:	*Journal of Analytical Atomic Spectrometry*
Manuscript ID	JA-ART-05-2018-000150.R1
Article Type:	Paper
Date Submitted by the Author:	05-Jul-2018
Complete List of Authors:	Lee, Yonghoon; Mokpo National University, Chemistry Mao, Xianglei; Lawrence Berkeley National Laboratory, Chan , George; Lawrence Berkeley National Laboratory Gonzalez, Jhanis; L. Berkeley National Lab, EETD; Applied Spectra, Russo, R; Lawrence Berkeley National Lab, Zorba, Vassilia; Lawrence Berkeley National Laboratory

SCHOLARONE™
Manuscripts

Spatial and Temporal Distribution of Metal Atoms and their Diatomic Oxide Molecules in Femtosecond Laser-Induced Plasmas

Yonghoon Lee,[a,b] Xianglei Mao,[a] George C.-Y. Chan,[a] Jhanis Gonzalez,[a,c] , Richard E. Russo[a,c] and Vassilia Zorba[a,*]

[a] Lawrence Berkeley National Laboratory, Berkeley CA 94720, United States.* E-mail: vzorba@lbl.gov

[b] Department of Chemistry, Mokpo National University, Jeonnam 58554, Republic of Korea

[c] Applied Spectra, Inc., 46665 Fremont Blvd., Fremont, CA 94538, United States

Abstract

We investigate the distribution of atoms and diatomic metal-oxide molecules in femtosecond laser-induced plasmas generated at and after the laser beam focal plane, where non-linear phenomena give rise to the formation of a weakly ionized air plasma channel. We use direct plasma imaging and optical emission spectroscopy to study plasma expansion, and the associated physical and chemical separation processes. Plasma splitting occurs upon the interaction of the weakly ionized plasma with the sample and is accompanied by a change in the spatio-temporal distribution of the molecules and atoms compared to sampling at the focus. Furthermore, molecular emission is favored at specific locations and is enhanced over atomic emission as the sample is moved underneath the laser focus. These findings support the ability to enhance or impede the formation of molecular versus atomic species at specific spatio-temporal locations in the laser-induced plasma.

1. Introduction

Controlling chemical reactions and separation processes in laser-induced plasmas has direct implications in laser ablation-based chemical analysis and is critical in tailoring the plasma composition. The spatio-temporal distribution of species in the expanding plasma is particularly important since it can affect what species are detected in optical emission and mass-spectrometry-based schemes. Laser ablation in air commonly leads to the formation of new molecular species, particularly oxides and nitrides, thereby adding to the complexity of the reactions taking place in the laser-induced plasma. The distribution of these species and resulting products is dependent on the laser parameters as well as on the ambient pressure. Although numerous studies have focused on physical characteristics like expansion dynamics, shockwave formation, plasma angular distribution in air, and other, much less is known about laser-induced plasma chemical reaction pathways and the spatio-temporal distribution of free atoms and molecules in it.[1,2,3] This is especially true in the femtosecond laser time regime, where molecular formation processes and their distribution remain largely unexplored.[4]

Molecular formation in laser-induced plasmas is influenced by several factors including molecular structure of solid samples[4,5] various reaction channels including direct ablation of molecules,[6] plasma expansion dynamics or mixing with ambient gas,[4] and combinations thereof.[7] Molecular signatures in laser plasmas provide useful information on the molecular structure of organic solids and have been successfully utilized for discrimination of polymers, biological species, and hazardous materials.[8,9,10] Furthermore, molecular band emission is the basis for laser-ablation molecular isotopic spectrometry (LAMIS) which enables isotopic analysis in laser-induced plasmas in real-time at atmospheric conditions.[11,12]

Femtosecond (fs) laser ablation sampling offers advantages such as suppressed thermal effects and high spatial and depth resolutions.[13,14,15] Femtosecond laser-induced plasmas are generally known to have lower temperature, shorter persistence time and are associated with suppressed thermal effects on the sample compared to those produced by nanosecond laser pulses.[16] While the majority of laser plasma optical emission investigations occur at the focal point of the lens focusing system, fs laser

ablation off-focus at positions after the lens focal plane (focal length of the lens) provides a pre-ionized medium above the sample. In the fs time regime, non-linear effects such as self-focusing and ionization can lead to the formation of a weakly ionized plasma channel.[17,18] This weakly ionized plasma channel in itself is a new source for ablation and plasma formation with characteristics distinctly different from those of focused femtosecond beams.

In this work, we use femtosecond weakly ionized plasma channels and focused femtosecond beams to study separation processes in the laser induced plasma. The weakly ionized plasma channel affects the shape and splitting of the expanding plasma from the titanium sample, as well as the distribution of molecules and free atoms. Although the formation of metal-oxide diatomic molecules in nanosecond laser induced plasmas has been investigated for TiO,[19,20,21,22] there is still very little known about TiO formation in tailored femtosecond laser induced plasmas. Herein, we study the spatial and temporal distribution of the plasma to find that the ratio of molecular-to-atomic species changes and that molecular formation is favored when ablating with the weakly ionized plasma channel. Moreover, the ratio of molecular-to-atomic species significantly depends on the distance from the femtosecond beam focus.

2. Experimental

A Ti:Sapphire femtosecond laser system (Astrella, Coherent) was used as the excitation source. The wavelength, pulse duration, pulse energy, and repetition rate were 800 nm, 35 fs, and 3.5 mJ/pulse, and 10 Hz, respectively. All experiments were performed at atmospheric pressure. The femtosecond laser beam was focused by a planoconvex lens (f = 150 mm and f-number = ~14). A titanium (Ti) metal target was used as a sample. The experiments were performed at six different sample height positions. Emission spectra were recorded with the sample surface located at the laser focal point (*IF*) and beyond to 2.5 (*OF1*), 3.2 (*OF2*), 3.9 (*OF3*), 4.6 (*OF4*), and 5.3 (*OF5*) mm underneath the laser focus respectively **(Figure 1)**. The laser irradiance on the sample surface for the different sample positions was IF : 6.6 x 10^{16}, OF1: 3.8x10^{14}, OF2: 2.3x10^{14}, OF3: 1.6x10^{14}, OF4: 1.1x10^{14} and OF5: 8.4x10^{13}

W/cm^2, respectively. A considerable part of the laser pulse energy is consumed even in the pre-focus region to generate continuum light, that propagates expanding into much larger solid angle than the femtosecond laser beam.[23] Also, the optical emission intensity is influenced by the mass ablated which is proportional to both crater area and ablation depth.

The femtosecond laser-induced plasma was imaged onto the entrance slit of a spectrometer (f = 1.25 m, Horiba JY 1250M) through two planoconvex lenses. The spectrometer was equipped with a 1200 grooves/mm grating and an intensified charge-coupled device detector (ICCD, PI-MAX, 1340 × 1300 pixels, 20 × 20 μm^2 pixel size). The plasma images were acquired from single laser pulses at various time delays, t, from the laser pulse, with the spectrometer set to its zeroth-order position. For these measurements, the ICCD detection gate width was set to 0.1 μs. Wavelength-resolved images were recorded with the grating centered at 708 and 393 nm. In the 708 nm range, TiO emission bands and Ti I lines could be detected simultaneously in the same spectral window. For excitation temperature calculations, Ti I lines in the wavelength region around 393 nm also were used. The ICCD detection gate widths were set to 0.2 and 1 μs, for t < 1 and ≥ 1 μs, respectively. For each spectrum, emission from 500 laser pulses was accumulated. During measurements, the Ti metal sample was translated by employing a motorized stage set at a speed of 1.0 mm/s.

3. Results and discussion

3.1. TiO distribution in fs laser-induced plasmas generated at the laser focus

Figure 2 shows time-resolved images of laser-induced plasmas generated by fs laser ablation of a Ti metal sample. For these images, the sample surface was located at the laser focal plane (indicated by "*IF*" in **Figure 1**). In agreement with previous findings, the angular distribution of the expanding femtosecond laser-induced plasma is relatively small as compared to a nanosecond pulsed laser plasma.[16,24] Reflection of the laser-induced plasma from the Ti metal surface (horizontal dotted line in **Figure 2**) is observed. **Figure 3** shows the LIBS emission spectrum measured under these conditions, at

1 μs delay. In the wavelength region between 705 and 715.5 nm, five Ti I emission lines (705.069, 706.521, 706.907, 713.030, and 713.890 nm)[25] and the TiO γ ($A\ ^3\Phi - X\ ^3\Delta$) $\Delta v = 0$ band[26] were assigned. The spectroscopic parameters of the five Ti I lines are listed in **Table 1**. In order to obtain temporal and spatial profiles of atomic and molecular emission intensities, the peak area between 704.941 and 705.141 nm around the Ti I line at 705.069 nm ($I_{\mathrm{Ti\ I}}$) and that between 705.328 and 705.829 nm around the TiO molecular band head at 705.429 nm (I_{TiO}) were integrated.

Figure 4 shows time-distance contour maps of (a) the atomic emission intensity of Ti, $I_{\mathrm{Ti\ I}}$ and (b) molecular emission intensity of TiO, I_{TiO}. These measurements were obtained when the sample was placed at the laser focal plane (i.e., position "*IF*"). As expected, oxide molecules tend to form later in time.[27,28] The majority of the atomic and molecular emission exists fairly close to the sample surface (< 2 mm), independent of the time after the laser pulse. This is consistent with the plasma images presented in **Figure 2**, in which the entire plasma emission is imaged onto the ICCD without element or molecule-specific emission information. The maximum intensity for the atomic emission is on the order of a few hundred nanoseconds after the pulse, versus 2 – 4 μs for molecular emission.

The ratio of molecular-to-atomic emission, $I_{\mathrm{TiO}}/I_{\mathrm{Ti\ I}}$ is shown in **Figure 4 (c)** as a function of distance for different delay times. This ratio increases with time, with a variation of up to an order of magnitude between early (~200 ns) and much later times (> 4 μs) from the laser pulse. Importantly, the reversible trend (initial decline followed by an overall rise) of the ratio as a function of distance reveals molecular-to-atomic signal enhancement close to the sample (0 mm) and toward the expanding front of the laser-induced plasma (2 mm). Clearly, TiO molecular emission is enhanced at both lower and higher ends of the plasma, similar to that measured with ns laser oxide formation in metals,[28] and has been attributed to lower temperature and effectiveness in mixing with ambient air at the outer parts (periphery) of the plasma.

3.2. TiO distribution in fs laser-induced plasmas from ablation after the laser focus

Figure 5 shows time-resolved emission images of fs laser-induced plasmas generated from the Ti metal sample with its surface at *OF2,* which *is* after *IF* by 3.2 mm (see **Figure 1**). An image of the weakly ionized plasma is shown on the left to demonstrate its relative position to that of the laser-induced plasma. The weakly ionized plasma image was measured using the same laser-focusing and imaging optics without the Ti metal sample in place. The ICCD detection gate (0.1 μs width) was delayed from the laser pulse by 0.1μs. The vertical length of the weakly ionized plasma channel is estimated to be 5 mm.

A physical separation of the laser-induced plasma is observed in **Figure 5.** This separation takes place at later delay times (indicated by the arrows), becoming prominent about 1 μs after the laser pulse. The upper plasma begins to expand toward the normal direction from the sample surface (into the weakly ionized plasma region) at around t = 0.33 μs. The separated upper plasma expanded up to ~1.5 mm from the top of the original plasma body with a speed of ~400 m/s. In comparison with the images taken at *IF*, shown in **Figure 2**, the total volume of the expanding plasma appears to be larger in the direction normal to the sample (vertical expansion). The total length of the combined plasma is roughly 3 mm at approximately 10 μs after the laser pulse. The physical separation of the plasma does not change significantly after ~4 μs. Separation has been previously observed in long-pulse laser-induced plasmas, particularly close to the Laser Supported Detonation Wave (LDSW) regime.[29] In the context of the existence of a pre-ionized medium, reports on orthogonal dual-pulse LIBS with a pre-ablation spark[30] indicated that the plasma can effectively expand into the pre-ablation spark zone located above it.

Figure 6 shows time-distance contour maps of $I_{\mathrm{Ti\ I}}$ (a) and I_{TiO} (b), and the ratio of $I_{\mathrm{TiO}}/I_{\mathrm{Ti\ I}}$ (c) obtained at *OF2* at different delay times. **Figure 6b** shows that there are two prominent lobes for TiO coinciding with the visible separation initiation time shown in **Figure 5**. After around t = 2 μs, the $I_{\mathrm{Ti\ I}}$ and I_{TiO} profiles show two clear peaks in their spatial profiles (see **Figures 6a** and **6b**). Note that the total intensity of emission in **Figure 6a** and **b** as indicated by the color scale of the contour plots are

lower than the case when the laser is in focus (**Figure 4**). This effect may be correlated, among others, with a reduced amount of mass ablated with lower total laser energy density reaching the sample.

The ratio of molecular to atomic emission in **Figure 6c** as a function of distance for different delay time, shows remarkable differences to that observed at the in-focus position (**Figure 4c**). Importantly, the formation of oxides versus atoms is enhanced significantly, especially at later times after the pulse. These data demonstrate that sampling configuration can be used to preferentially drive the formation of molecules in laser induced plasmas.

Figure 7a shows the temperature profiles for the fs laser-induced plasma with the sample surface at *IF* and *OF2*. Ti shows well-known strong atomic emission lines in near ultraviolet wavelength region.[31] Among them, two Ti I lines at 391.118 and 392.142 nm were chosen for the determination of temperature. The spectroscopic parameters of these two Ti I lines are listed in **Table 1**. The excitation temperature, *T*, as a function of distance at each sample position was evaluated using the Boltzmann plot method:

$$T = -\frac{(E_i - E_m)}{k} \frac{1}{\ln\left(I_{ij} A_{mn} g_m / I_{mn} A_{ij} g_i\right)} \quad (1)$$

where E_i and E_m are the upper-level energies of the Ti I lines at 391.118, and 392.142 nm, I_{ij}, A_{ij}, and g_i are the measured intensity, the transition probability, and the upper-level statistical weight for the Ti I line at 391.118 nm, respectively. I_{mn}, A_{mn}, and g_m are the corresponding parameters for the 392.142 nm Ti I line. *k* represents the Boltzmann constant.

We found that the excitation temperature is consistently lower for *OF2* than for *IF* (**Figure 7a**). A local minimum in temperature at around 1 mm coincides with the physical separation of the plasma at around 1 – 2 μs after the pulse, in which the boundary of the two split plasmas is also located at approximately 1 mm (cf. **Figure 5**). Several factors may influence TiO molecular formation, including temperature and mixing of the Ti plasma with O_2 supplied by ambient air. If the two reactants were mixed homogeneously, TiO formation would follow the trend expected based on temperature leading to enhanced molecule formation as temperature decreases. However, the molecular to atomic ratio ($I_{TiO}/I_{Ti\,I}$)

integrated between 1 to 2 μs shown in **Figure 7b** does not follow the expected trend based on the temperature profile shown in **Figure 7a**. The lower $I_{TiO}/I_{Ti\ I}$ values were observed at the positions where the lower temperature was measured. This suggests the existence of other mechanisms responsible for oxide formation. One possible mechanism is mixing of the Ti plasma with ambient air. Assuming incomplete mixing, TiO formation can be facilitated mostly on the periphery of the plasma. This would explain the increase at bottom and top edges of the $I_{TiO}/I_{Ti\ I}$ profiles. In the course of plasma cooling with time, temperature decreases and the Ti plasma and the ambient air are mixed more thoroughly, which can also accelerate the temperature decrease, because the ambient air is colder than the plasma. This may contribute to the higher $I_{TiO}/I_{Ti\ I}$ and fairly constant vs. distance ratio at longer delay times (**Figure 6c)**. The hydrodynamic flow and relative pressure of oxygen and its interaction with the laser-induced plasma is expected to play a key role in the formation of oxides and their distribution in the plasma. The laser ablation process is accompanied by complex shockwave dynamics, plasma expansion and pressure gradients with the existence of rarified regions. Excitation, photodissociation, and ionization processes in air also play an important role. The relative contribution of each individual mechanism in the formation of the molecular species versus atomic, and their distribution in the laser-induced plasma are complex, and dedicated work is required to elucidate mechanisms in this new unexplored regime of fs weakly ionized plasma channels on ablation and plasma behavior.

3.3. Effect of sample position and weakly ionized plasma on TiO formation

The $I_{Ti\ I}$ and I_{TiO} profiles as a function of distance, obtained for the six sample positions in focus and out-of-focus (weakly ionized plasma channel regime), are compared in **Figure 8a.** Maximum emission intensity for both $I_{Ti\ I}$ and I_{TiO} was observed when the sample surface was located at the laser focus (*IF*). As the sample was moved to greater distances from the focus, $I_{Ti\ I}$ decreased rapidly. This decrease may be attributed to the decrease in laser energy density delivered to the sample as it is moved away from the focus, leading to a decrease in the amount of ablated mass and the plasma excitation temperature. However, the variation of I_{TiO} with the sample position is significantly different from that of $I_{Ti\ I}$, while

I_{TiO} decreased from *IF* to *OF1*, further lowering the sample surface from the focus led to an increase in I_{TiO}.

Figure 8b shows the $I_{TiO}/I_{Ti\ I}$ profiles, for the different sample positions as a function of distance from the sample surface. In the middle of the $I_{TiO}/I_{Ti\ I}$ profiles for *OF3*, *OF4*, and *OF5*, there are clear increases of $I_{TiO}/I_{Ti\ I}$. The location of each increase agrees well with the corresponding position of the gap between the two split plasmas. This increase in $I_{TiO}/I_{Ti\ I}$ in the middle of the plasma is much less pronounced in *OF1* and *OF2,* and starts becoming much more significant and with a wider distribution when the sample surface was lowered further (*OF3*-*OF5*). Therefore, the gap between the two plasmas seems to have a crucial influence on the TiO molecular formation.

TiO molecules can be formed through the following two reaction routes:

$$Ti + O_2 \leftrightarrow TiO + O \qquad (2)$$

$$\begin{aligned} O_2 + M &\leftrightarrow O + O + M \\ Ti + O &\leftrightarrow TiO \end{aligned} \qquad (3)$$

In equation (3), *M* represents a partner of O_2 for the given inelastic collision resulting to dissociation of O_2. Under equilibrium, an increase in the partial pressure of O_2, one of the reactants, leads to an enhancement of TiO formation in both routes shifting the equilibrium toward reactants. The gap between the two plasmas may provide an additional plasma zone to interact with ambient air and supply oxygen to form molecules, and further account for the decrease in the plasma excitation temperature (see position of the temperature profile of *OF2* indicated by the arrow in **Figure 7a)**.

Figure 8c shows the spatially averaged $I_{TiO}/I_{Ti\ I}$ as a function of distance above the sample. An exponential increase of the molecular-to-atomic ratio is observed as the sample surface is moved away from *IF*. This result may demonstarte a direct correlation of molecular formation with the laser irradiance on the sample surface. However, the promotion of molecular formation should be interpreted as a consequence of complicated underlying processes, as described in detail in the previous section. These measurements demonstrate that molecular to atomic spatial emission is related to the distance between the weakly ionized and surface plasmas. Furthermore, these experiments show the ability to

control the TiO molecular formation during the expansion of the femtosecond laser-induced plasmas by tailoring the interaction with the weakly ionized plasma channel.

4. Conclusion

We studied the spatio-temporal distribution of Ti and TiO molecules in plasmas produced using femtosecond laser beams in- and out-of-focus (weakly ionized plasma channel regime), using optical emission spectroscopy. We found that plasma splitting processes take place upon the interaction of the weakly ionized plasma with the sample. This phenomenon was accompanied by changes in the distribution of atomic and molecular species in the plasma. A significant enhancement of the molecular-to-atomic emission was observed using weakly ionized plasma channels versus a focused femtosecond beam, and this ratio can be controlled by adjusting the position of the sample with respect to the weakly ionized plasma channel. These findings also provide insight into the spatio-temporal distribution of metal-oxide molecules in femtosecond laser-induced plasmas generated in air, which can be used to facilitate tailored plasma chemistries by enhancing or impeding molecular versus atomic species formation.

Acknowledgements

This research was supported by the US Department of Energy, Office of Defense Nuclear Nonproliferation Research and Development under contract number DE-AC02-05CH11231 at the Lawrence Berkeley National Laboratory.

References

1 M. Dong. G.C.-Y. Chan, X. Mao, J.J. Gonzalez, J. Lu, R.E. Russo, Elucidation of C2 and CN formation mechanisms in laser-induced plasmas through correlation analysis of carbon isotopic ratio, *Spectrochim. Acta B,* 2014,**100**, 62.

2 P. Lucena, A. Dona, L.M. Tobaria, J.J. Laserna, New challenges and insights in the detection and spectral identification of organic explosives by laser induced breakdown spectroscopy, *Spectrochim. Acta B*, 2011, 66, 12.

3 X. Baia, V. Motto-Ros, W. Lei, L. Zheng, J. Yu, Experimental determination of the temperature range of AlO molecular emission in laser-induced aluminum plasma in air, *Spectrochim. Acta B*, 2014, **99**, 193.

4 J. Serrano, J. Moros and J. Laserna, Exploring the Formation Routes of Diatomic Hydrogenated Radicals Using Femtosecond Laser-Induced Breakdown Spectroscopy of Deuterated Molecular Solids, *J. Anal. At. Spectrom.*, 2015, **30**, 2343.

5 Á. Fernández-Bravo, T. Delgado, P. Lucena, J. Laserna, Vibrational emission analysis of the CN molecules in laser-induced breakdown spectroscopy of organic compounds, *Spectrochim. Acta B*, 2013, **89**, 77–83.

6 R. Saad, D. L'Hermite and B. Bousquet, Unexpected temporal evolution of atomic spectral lines of aluminum in a laser induced breakdown spectroscopy experiment, *Spectrochim. Acta B,* 2014, **101** 330–334.

7 R. Glaus, J. Riedel, and I. Gornushkin, Insight into the Formation of Molecular Species in Laser-Induced Plasma of Isotopically Labeled Organic Samples, *Anal. Chem.* 2015, **87**, 10131−10137.

8 M. Baudelet, M. Boueri, J. Yu, S.S. Mao, V. Piscitelli, X. Mao, R.E. Russo, Time-resolved ultraviolet laser-induced breakdown spectroscopy for organic material analysis, *Spectrochim. Acta B*, 2007, **62,** 1329–1334.

9 S. J. Rehse, H. Salimnia and A. W. Miziolek, Laser-induced breakdown spectroscopy (LIBS): an overview of recent progress and future potential for biomedical applications, *J. Med. Eng. Technol.*, 2012, **36**, 77–89.

10 J. L. Gottfried, F. C. De Lucia Jr, C. A. Munson, A. W. Miziolek, Laser-Induced Breakdown Spectroscopy for Detection of Explosives Residues: A Review of Recent Advances, Challenges, and Future Prospects, *Anal. Bioanal. Chem.* 2009, **395**, 283

11 R.E. Russo, A.A. Bol'shakov, X. Mao, C.P. McKay, D.L. Perry, and O. Sorkhabi. "Laser ablation molecular isotopic spectrometry", *Spectrochim. Acta B*, 2011, **66(2**), 99-104.

12 A. A. Bol'shakov, X. Mao, J. J. González and R. E. Russo, Laser Ablation Molecular Isotopic Spectrometry (LAMIS): Current State of the Art, *J. Anal. At. Spectrom.*, 2016, **31**, 119.

13 D. von der Linde and K. Sokolowski-Tinten, The physical mechanisms of short-pulse laser ablation, *Appl. Surf. Science* 2000, **154-155,** 1-10.

14 D. Bäuerle, *Laser Processing and Chemistry*; Springer: Berlin (2000).

15 V. Zorba, X. Mao and R.E. Russo, Femtosecond Laser Induced Breakdown Spectroscopy of Cu at the micron/sub-micron scale, *Spectrochim. Acta B* **113**, 37 (2015).

16 R.E. Russo, X.L. Mao, J.J. Gonzalez and J. Yoo, Femtosecond Versus Nanosecond Laser Pulse Duration for Laser Ablation Chemical Analysis, *Spectroscopy,* 2013, **28**, 24.

17 G. Point, C. Milián, A. Couairon, A. Mysyrowicz, A. Houard , Generation of long-lived underdense channels using femtosecond filamentation in air*, J. Phys. B: At. Mol. Opt. Phys*., 2015, **48**, 094009

18 H. Hou, X.L. Mao, V. Zorba, R. E. Russo, Laser Ablation Molecular Isotopic Spectrometry for Molecule Formation Chemistry in fs-Laser Ablated Plasmas, *Anal. Chem.* 2017, **89**, 750.

19 A. De Giacomo, V. A. Shakhatov, and O. De Pascale, Optical Emission Spectroscopy and Modeling of Plasma Produced by Laser Ablation of Titanium Oxides, Spectrochim. Acta Part B, 2001, 56, 753-776.

20 A. De Giacomo, Experimental Characterization of Metallic Titanium-Laser Induced Plasma by Time and Space Resolved Optical Emission Spectroscopy, Spectrochim. Acta Part B, 2003, 58, 71-83.

21 A. De Giacomo, M. Dell'Aglio, A. Santagata, and R. Teghil, Early Stage Emission Spectroscopy Study of Metallic Titanium Plasma Induced in Air by Femtosecond- and Nanosecond-laser pulses, Spectrochim. Acta Part B, 2005, 60, 935-947

22 A. C. Woods and C. G. Parigger, Diatomic Molecular Emission Spectroscopy of Laser-Induced Titanium Plasma, J. Phys.: Conf. Ser. 2014, 548, 012037.

23 C. A. Zuhlke, J. Bruce III, T. P. Anderson, D. R. Alexander, and C. G. Parigger, A Fundamental Understanding of the Dependence of the Laser-Induced Breakdown Spectroscopy (LIBS) Signal Strength on the Complex Focusing Dynamics of Femtosecond Laser Pulses on Either Side of the Focus, *Appl. Spectrosc.* 2014, 68, 1021-1029.

24 J.R. Freeman, S.S. Harilal, P.K. Diwarkar, B. Verhoff, A. Hassanein, Comparison of Optical Emission from Nanosecond and Femtosecond Laser Produced Plasma in Atmosphere and Vacuum Conditions. *Spectrochim. Acta Part B,* 2013, **87**, 43-50.

25 NIST Atomic Spectra Database

26 J.G. Phillips, Molecular constants of the TiO molecule, *The Astrophysical Journal Supplement Series,* 1973, **232-26**, 313-331.

27 V. S. Burakov, N. A. Savastenko, and N. V. Tarasenko, Formation of chemical compounds in a laser plasma, *J. Appl. Spectrosc.*, 1999, **66**,15.

28 J. Lam, V. Motto-Ros, D. Misiak, C. Dujardin, G. Ledoux and D. Amans, Investigation of Local Thermodynamic Equilibrium in Laser-induced Plasmas: Measurements of Rotational and Excitation Temperatures at Long Time Scales, *Spectrochim. Acta B*, 2014, **101**, 86.

29 N. M. Bulgakova, A.N. Panchenko, V.P. Zhukov, S. I. Kudryashov, A. Pereira, W. Marine, T. Mocek and A.V. Bulgakov, "Impacts of Ambient and Ablation Plasmas on Short- and Ultrashort-Pulse Laser Processing of Surfaces", *Micromachines,* 2014, ***5***, 1344.

30 S.-C. Choi, M.-K. Oh, Y. Lee, S. Nam, D.-K. Ko and J. Lee, "Dynamic effects of a pre-ablation spark in the orthogonal dual-pulse laser induced breakdown spectroscopy", *Spectrochim. Acta B*, 2009, **64,** 427–435.

31 D. A. Cremers and L. J. Radziemski, *Handbook of Laser-Induced Breakdown Spectroscopy*, Wiley, West Sussex,1st edn, 2006. pp. 5.

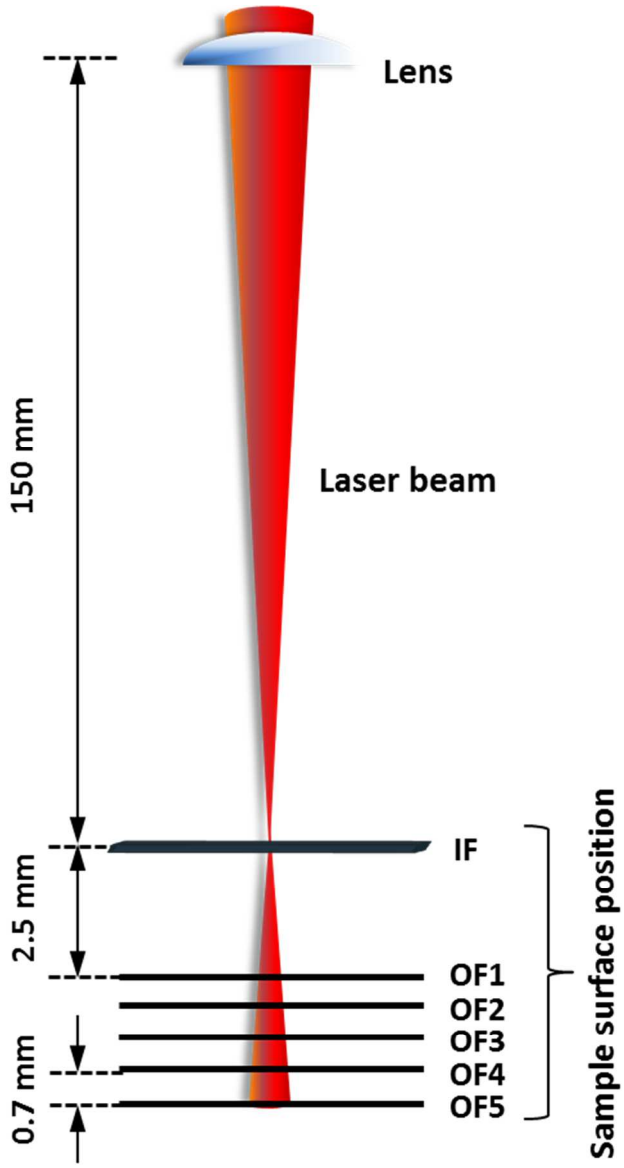

Figure 1. Six different positions of the sample surface relative to the laser focus. *"IF"* indicates the sample surface position at the focus of a laser beam (15 mm from the focusing lens). The other positions indicated by *"OF1", "OF2", "OF3", "OF4",* and *"OF5"* are after the laser focus.

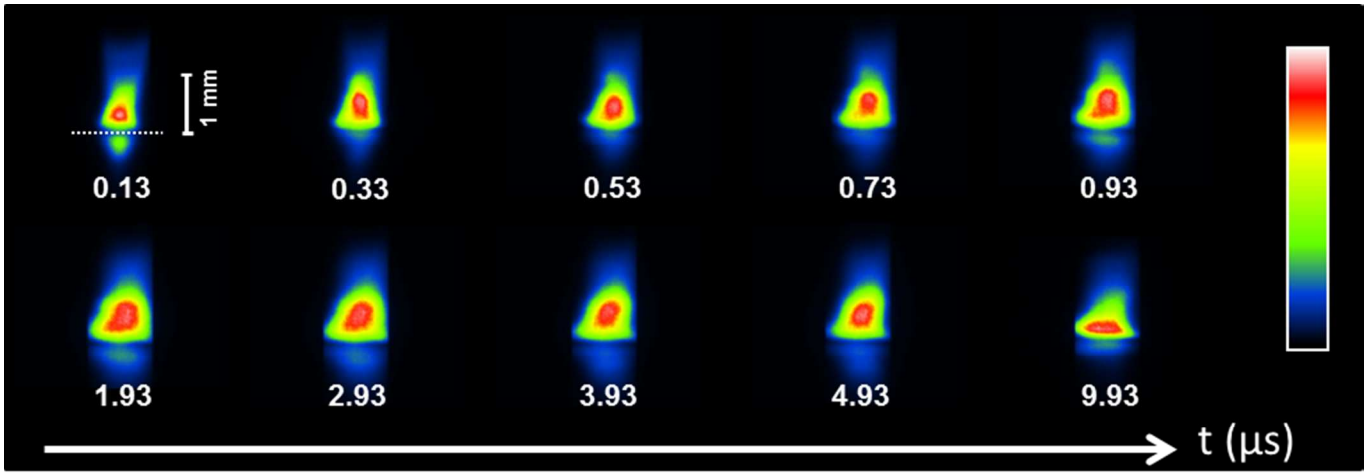

Figure 2. Time-resolved images of fs laser-induced plasmas generated during ablation of a Ti sample positioned at the laser focus (indicted as *"IF"* in **Figure 1**). For each image, a delay time (in μs) from the laser pulse is noted. The horizontal dotted line indicates the sample surface position. Observed emission under the sample surface is due to reflection from the Ti metal. The color scale represents the minimum and maximum intensity of each individual plasma emission frame.

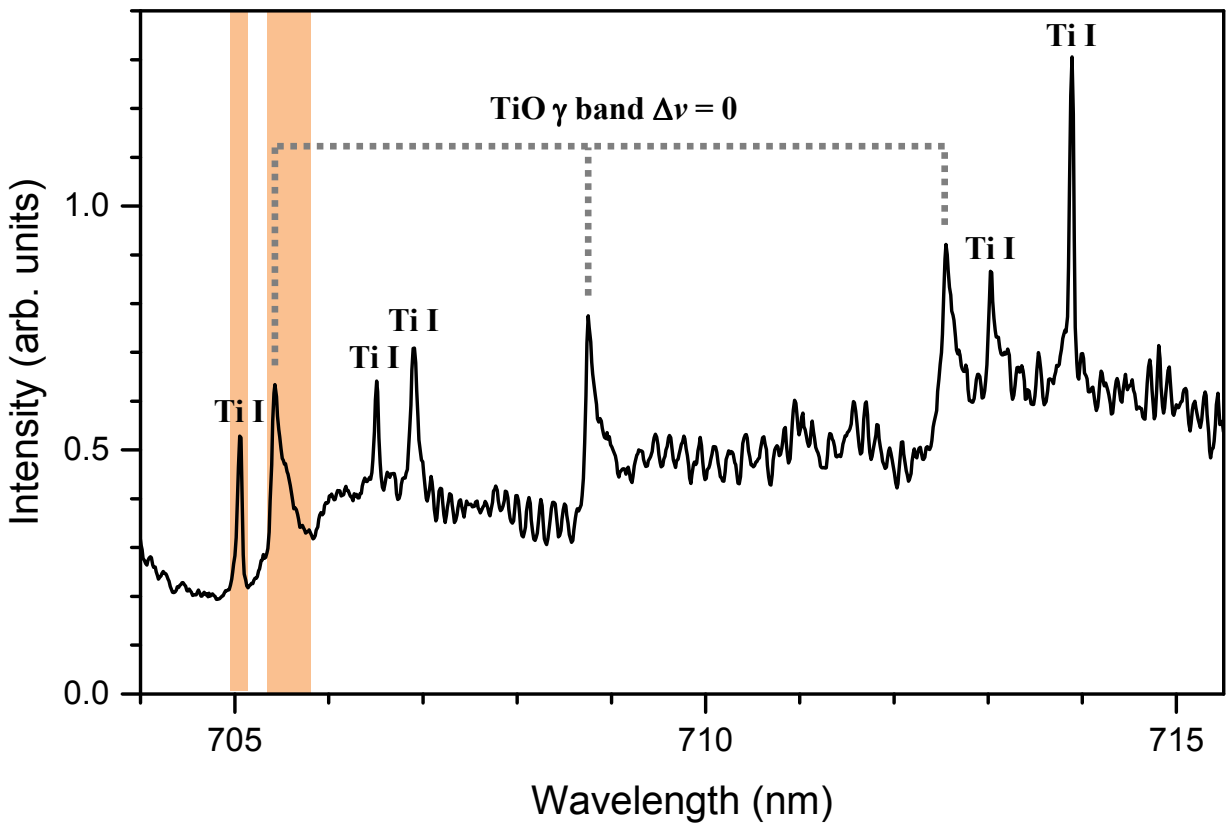

Figure 3. LIBS spectrum recorded for sample surface position in focus *(IF)* showing the Ti I emission lines and the TiO γ band $\Delta v = 0$. The highlighted Ti I line at 705.069 nm and the TiO molecular band head at 705.429 nm were used for comparing atomic line and molecular band intensities. The ICCD detection gate was delayed from the laser pulse by 1 μs and its width was set to 1 μs.

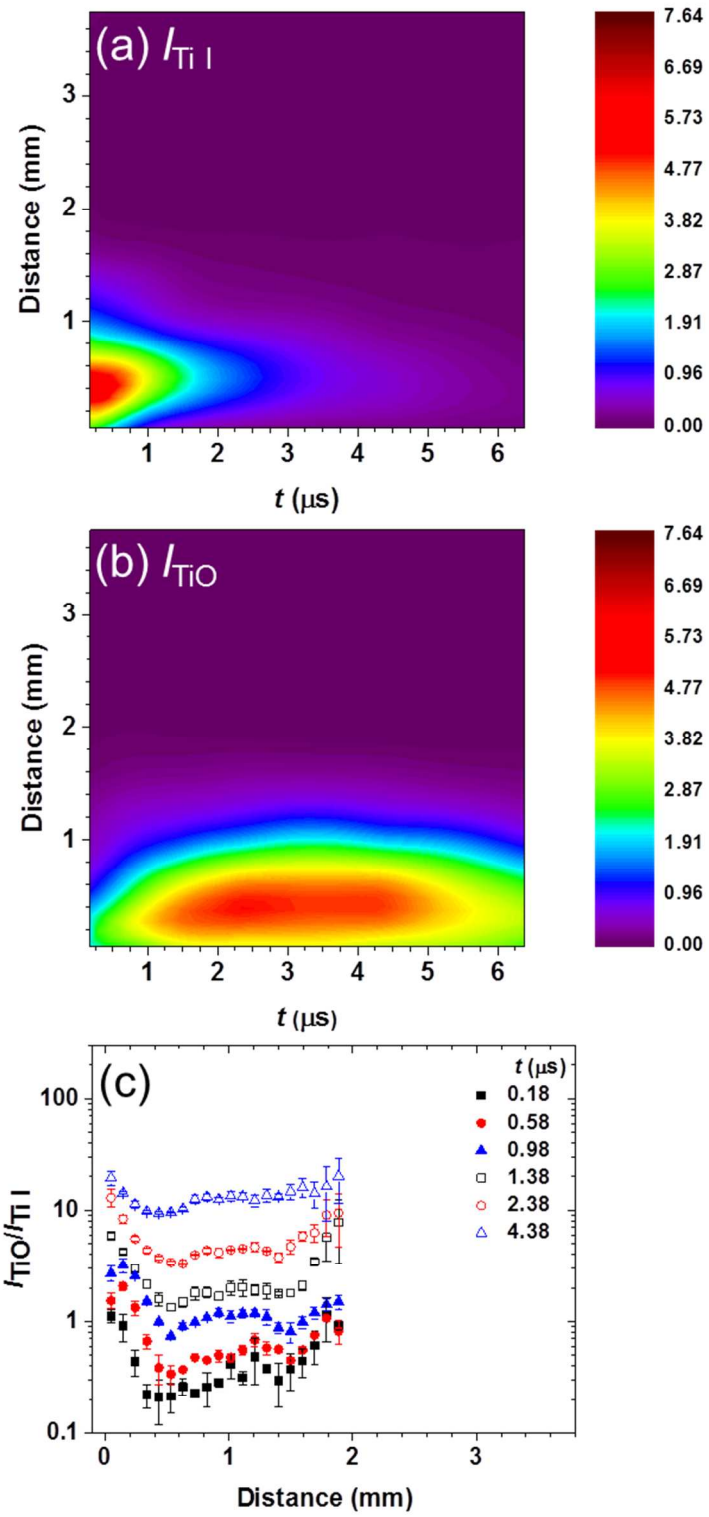

Figure 4. Distance-time contour maps of (a) $I_{Ti\ I}$ and (b) I_{TiO} intensities obtained for sample position, *IF* (c) The ratio of $I_{TiO}/I_{Ti\ I}$ as a function of distance for different delay times, *t*. For shorter delay times, $t <$ 1 μs, the ICCD detection gate width was set to 0.2 μs. For the longer $t \geq 1$ μs, the gate width was set to 1 μs. Distance 0 is at the sample surface.

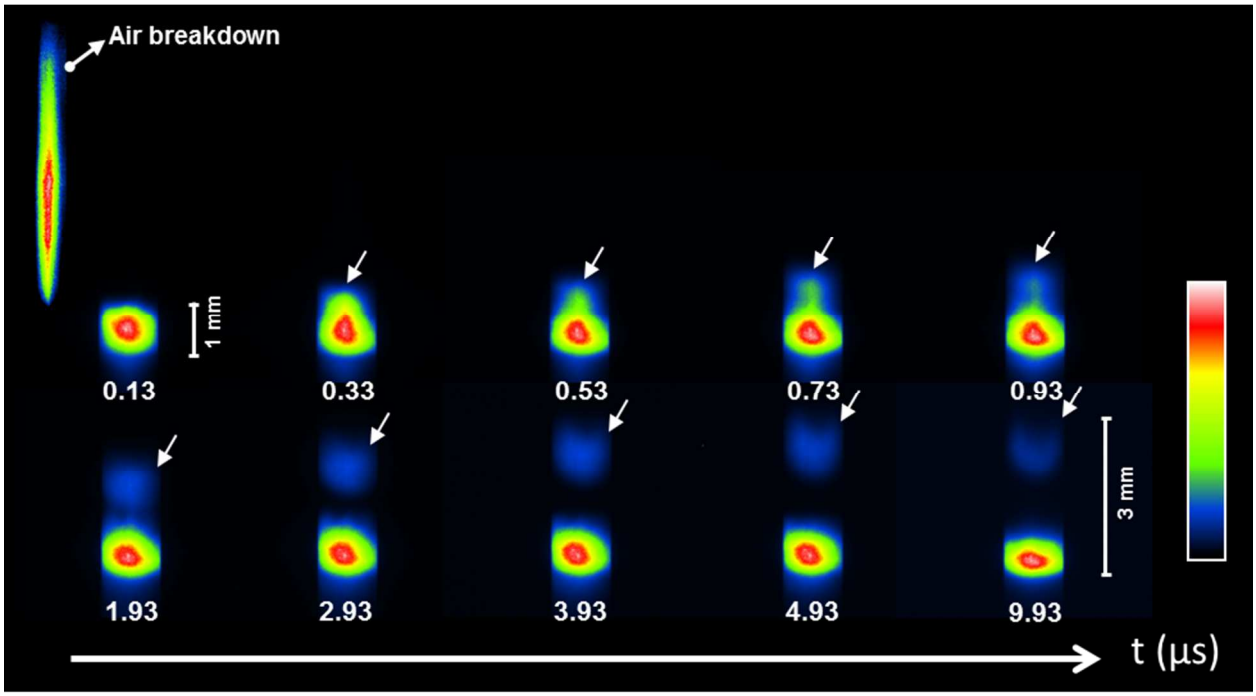

Figure 5. Time-resolved images of femtosecond laser-induced plasmas generated at off-focus sample surface positions, *OF2*. For each image, the delay time from the laser pulse, *t*, is noted in μs. The air-breakdown image is presented to show its position relative to the plasma originating from the sample surface. All emission images were taken using the same imaging lenses for the sample plasma images. The arrows indicate separation and expansion of the upper part of the sample plasma. The color scale represents the minimum and maximum emission intensity of each individual plasma frame.

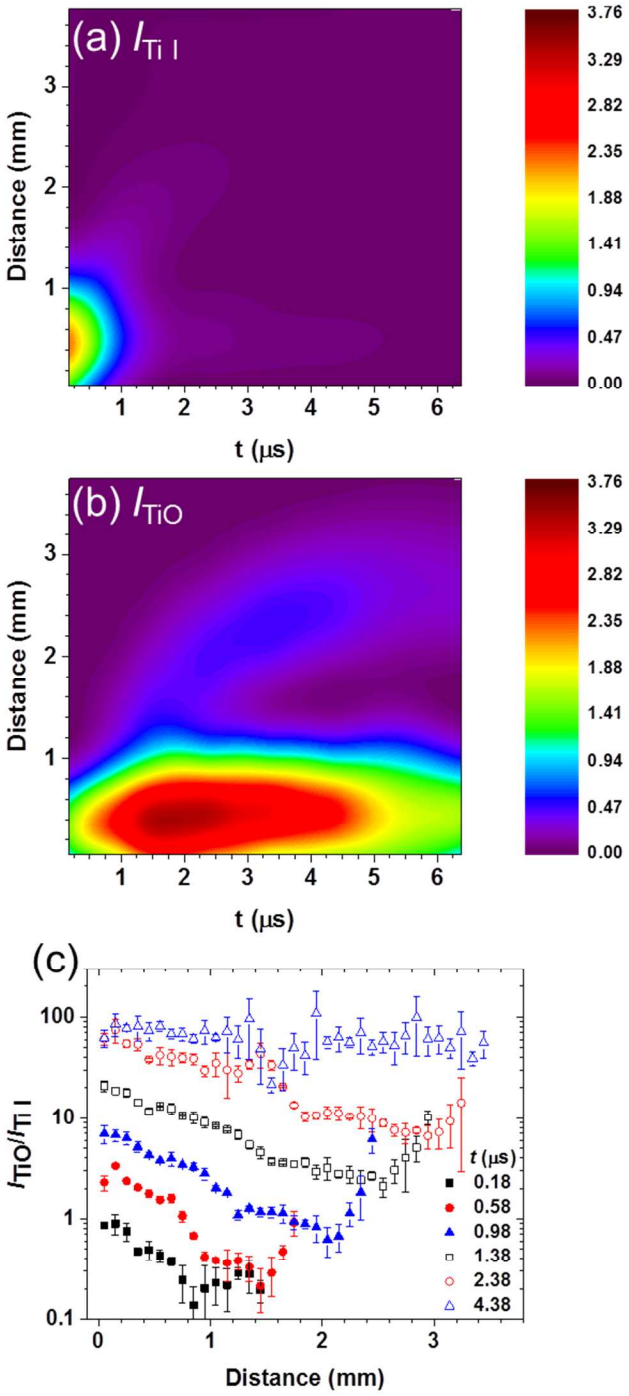

Figure 6. Distance-time contour maps of (a) $I_{Ti\ I}$ and (b) I_{TiO} emission intensities obtained for sample position, *OF2* (3.2 mm after the laser focus) (c) The ratio of $I_{TiO}/I_{Ti\ I}$ as a function of distance for different delay times, t. For shorter delay times, $t < 1$ μs, the ICCD detection gate width was set to 0.2 μs. For the longer $t \geq 1$ μs, the gate width was set to 1 μs.

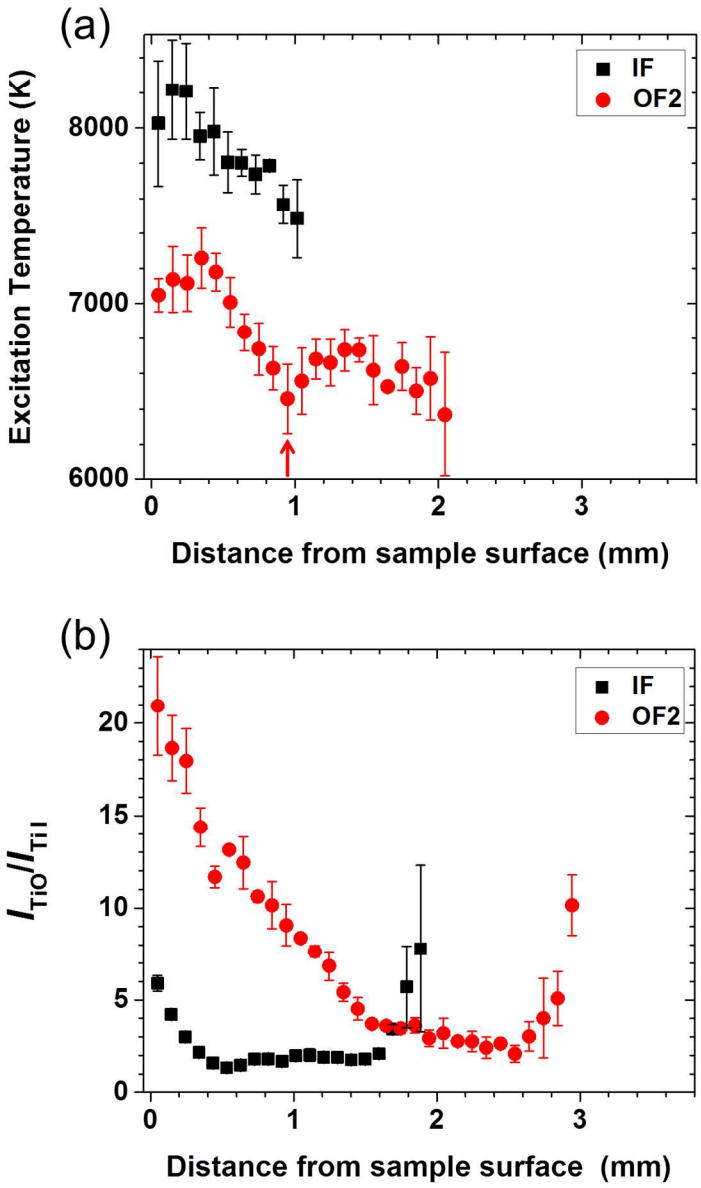

Figure 7. (a) Plasma temperatures determined using two Ti I lines intensities at 391.118 and 392.142 nm for sample surface positions, *IF* and *OF2*. (b) The corresponding TiO/Ti I intensity ratio as a function of distance from the sample surface. The ICCD detection gate was delayed from the laser pulse by 1 μs and its width was set to 1 μs.

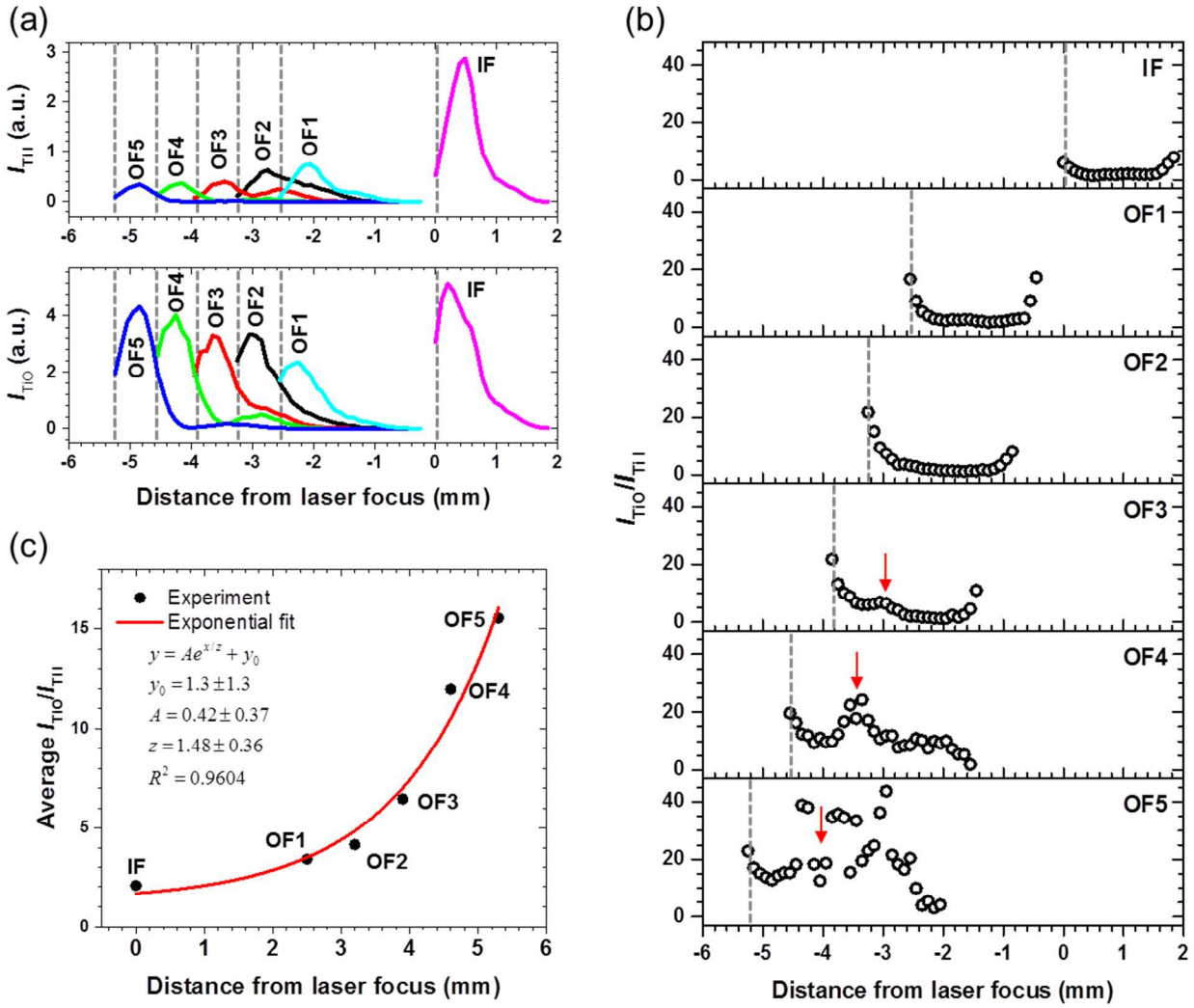

Figure 8. Atomic and molecular emission at different distances from the laser focus: (a) $I_{\mathrm{Ti\,I}}$ and I_{TiO} profiles as a function of distance, (b) $I_{\mathrm{TiO}}/I_{\mathrm{Ti\,I}}$ profiles spatially and (c) averaged $I_{\mathrm{TiO}}/I_{\mathrm{Ti\,I}}$ ratio. In (a) and (b), the vertical dashed lines indicate the sample surface positions. The arrows in (b) show the gap positions between the two split parts of the fs laser-induced plasma for *OF3, OF4*, and *OF5*. These data were obtained with a 1-μs ICCD detection gate width delayed from the laser pulse by 1 μs.

Wavelength (nm)	$A_{\text{upper-lower}}$ (s^{-1})	E_{lower} (cm^{-1})	E_{upper} (cm^{-1})	g_{lower}	g_{upper}
705.0686		18911.394	33090.497	5	3
706.5210		11776.812	25926.771	9	9
706.9073		25643.701	39785.923	7	9
713.0303		11776.812	25797.595	9	7
713.8903	4.8×10^{5}	11639.8109	25643.701	7	7
391.11849	1.83×10^{7}	16458.671	42019.129	13	13
392.14225	2.48×10^{6}	0.000	25493.733	5	5

Table 1. Spectroscopic parameters of the Ti I lines observed in the wavelength between 705 and 715.5 nm and those in the ultraviolet region utilized for plasma temperature determinations.